Permselectivity improvement in membranes for CO2/N2 separation

Ana Fernández-Barquín1, Clara Casado-Coterillo, Miguel Palomino, Susana Valencia, Angel Irabien

Separation and Purification Technology

VOLUME: 157

Page: 102-111

2016

http://dx.doi.org/10.1016/j.seppur.2015.11.032

Permselectivity improvement in membranes for CO_2/N_2 separation

Ana Fernández-Barquín[1,*], Clara Casado-Coterillo[1], Miguel Palomino[2], Susana Valencia[2], Angel Irabien[1]

[1] *Department of Chemical and Biomolecular Engineering, ETSIIT, Universidad de Cantabria, Av. Los Castros s/n, 39005 Santander (Cantabria) SPAIN*

[2] *Institute of Chemical Technology, UPV-CSIC, Av. Naranjos s/n, 46022 Valencia, SPAIN*

*Corresponding author: fbarquina@unican.es; Tel. +34 942 206777; Fax: +34 942 201591

Keywords

Mixed-matrix membranes; temperature; small-pore Si/Al=5 zeolites; PTMSP; CO_2/N_2 separation

Abstract

In this work, small-pore zeolites of different topology (CHA, LTA5, Rho), all with Si/Al ratio of 5, have been added to highly permeable poly(1-trimethylsilyl-1-propyne) (PTMSP) to increase its selectivity and thermal and mechanical stability. Membranes were characterized by TGA, XRD, SEM and CO_2 and N_2 single gas permeation measurements at different temperatures. TGA reveal that the thermal resistance of the membranes is as good as pure PTMSP polymer. XRD and SEM results reflect that there is good interaction between the fillers and the membrane matrix, at 5 and 10 wt. % zeolite

loadings, while at 20 wt.% a dual layer stucture is formed, when Rho zeolite is the filler, because the particle size of Rho is higher than those of LTA5 or CHA, and voids appear that limit the permselectivity performance. In single gas permeation of N_2 and CO_2, the influence of temperature, zeolite loading and type is analyzed. The selectivity of pure PTMSP is considerably enhanced with the addition of the zeolites and the increase of temperature, and the MMM loaded with 5 wt. % zeolite surpassed the Robeson's upper bound for CO_2/N_2 separation, without decreasing the permeability too much. Upon increasing temperature from 298 to 333 K, the permselectivity is enhanced even further without loss of permeability. The 5 wt% loaded membranes were tested in CO_2/N_2 mixed gas separation experiments at 333 K and 12.5 wt. % CO_2 in the feed, and the permselectivity of LTA5- and Rho-PTMSP membranes was further enhanced, compared with the single gas permeation experiments.

1. Introduction

The atmospheric concentration of greenhouse gases (GHGs) has increased significantly over the last century [1]. Carbon dioxide is the main component of these gases, and its accumulation in the environment is leading to severe global warming issues, which makes necessary finding a feasible separation technology for the removal of CO_2 from flue gases. Membrane technology appears to be an attractive option in terms of energy saving, modularity, ease of scaling up and control [2], such as those energy intensive based on wet scrubbing using aqueous amine solutions [3]. In a typical coal-fired power plant the flue gas is about 323 K, nearly at atmospheric pressure, and has a CO_2 content as low as 10 – 15 % and partial pressure of 10 – 15 kPa [4]. Therefore, membranes with high CO_2 permeability and moderate selectivity over other gases are required in order to allow working in a wider range of operating conditions in post-

combustion [5]. Besides, membranes should present good thermal and mechanical properties and be robust enough for long term operation [6]. In particular, the impact of membrane material in CO_2 removal is as important as the process conditions [7].

Polymeric membranes appear, currently, to be the most advanced option for membrane-based post-combustion carbon capture in terms of CO_2/N_2 permselectivity [8]. However, the lack of thermal stability or inadequate performance in terms of permselectivity limit their use in industrial separations. In fact, there is a well-known trade-off between selectivity and permeability for a specific pair of gases separation [9]. One of the ways of improving the performance of polymer membranes is based on the concept of mixed-matrix membranes (MMM), which combine the molecular sieving effect and other properties of the dispersed fillers with the processing feasibility of polymeric materials to achieve a new material with enhanced mechanical and functional properties [10]. Components selection is a key feature in the development of new mixed matrix membranes. A good adhesion between polymer and sieve is a factor of paramount importance in order to achieve a defect-free MMM with synergic properties, and this limits the choice of candidate materials [11].

Since polymer selection determines the minimum separation performance, poly (1-trimethylsilyl-1-propyne) (PTMSP), which is the organic polymer with the highest gas permeability reported, being located at the right of the Robeson's upper bound [9], is selected as continuous matrix in this work, since it. The CO_2 permeability of PTMSP reported in literature covers a range between 16000 – 38000 Barrer at 298 K [12, 13], probably because the different stages of aging affecting PTMSP performance [14]. The high permeability of PTMSP is based on high solubility and high diffusivity and is probably related to its very low density (0.75 g cm^{-3}) and its extremely high free volume (0.29) [15, 16], accounting for the presence of microvoids [12], compared with the rest

of dense glassy polyimides [17]. The glassy structure of PTMSP explains the low chain mobility with a glass transition temperature greater than 523 K [15], which makes it a promising material for high temperature membrane separations, but leads to loss of permselectivity with time due to physical aging phenomena upon permeation and CO_2 plasticization. The addition of properly selected inorganic fillers is supposed to enhance membrane selectivity when no defects are presented [18-20].

Zeolites were the first molecular sieves used as fillers in polymer matrices for gas separation because of their crystalline character with well-defined pore structures and shape selectivity properties [21]. Zeolite 4A nanoparticles have been widely reported in the literature to increase the permselectivity performance of glassy polyimides such as Matrimid [22], P84 [23], polyvinyl acetate [24], polycarbonate [25], or poly ether sulfone (PES) [26], and rather constant selectivity. However, adhesion with the commercially available polymers mentioned above is still a major challenge and many efforts have been made regarding preparation methods such as priming [26], zeolite modification by organic linkers [27] or zeolite preheat treatment [28]. Besides, zeolite 4A with a Si/Al ratio of 1 is very sensitive to the presence of moisture, which is a main component in flue gas, constituting a problem because the adsorbed water may not be easily released at the membrane separation temperatures [28]. The effect of Si/Al ratio on LTA fillers in PTMSP for CO_2/N_2 separation was studied in a previous work, using zeolites with Si/Al ratio 1 (Zeolite A) and ∞ (ITQ-29) [29]. The membranes prepared with low-Si/Al ratio showed the highest CO_2 permeability and selectivity, surpassing Robeson's upper bound even at 333 K, due to better adhesion between zeolite A and the polymer matrix, obtaining a dual layer structure that approach the membrane performance to that of a pure zeolite A membrane at 20 wt. % zeolite A loading. Pure silica ITQ-29 did not dispersed or adhered too well with the rigid structure of the super glassy PTMSP polymer [30]. The

ideal CO_2 adsorbent is a material with an intermediate CO_2 affinity, high adsorption capacity, combined with good selectivity and easy regeneration. This applies also for an effective filler for CO_2 selective MMM. Kosinov et al. [31] have just presented promising CHA (SSZ-13) purely inorganic hollow fiber CO_2 selective membranes but they did not manage a Si/Al ratio as high as 5 into a defect-free zeolite layer. In the particular case of PTMSP, as far as we know, only Woo et al. [20] and Fernández-Barquín et al. [29] employed porous zeolites to modify the gas separation performance of the PTMSP. As far as we know, no works have yet been reported employing CHA or Rho zeolites into a mixed matrix membrane using PTMSP.

This is the reason why, in this work, we study the effect of small-pore zeolites with Si/Al ratio of 5 and different structures (CHA, LTA5 and Rho), as well as good CO_2 adsorbing capacity, on the PTMSP matrix for MMM performance in CO_2/N_2 separation. MMM were characterized by thermogravimetric analysis (TGA), scanning electron microscopy (SEM), X-ray diffraction (XRD), and pure gas permeation of N_2 and CO_2, in the temperature range of 298 – 333 K, taking into account the mechanical and thermal stability. The most promising membranes were also measured in dry 12.5% CO_2/ 87.5% N_2 mixture separation at 333 K, to evaluate gas separation performance.

2. Experimental

2.1 Preparation of MMM

MMM were prepared following the procedure described in our previous work [29]. Poly (trimethylsilyl propyne) (PTMSP) was purchased from ABCR GmbH (Germany) with a purity of 95%, dried at 70 ºC for several hours before being dissolved

in toluene. The difference is that in this work, the zeolite fillers employed have different topologies, CHA, LTA and Rho.

Zeolites were synthesized at the Instituto de Tecnología Química in Valencia, according to procedures reported in literature [32, 33, 34], with a Si/Al molar ratio of 5 and the properties that are summarized in **Table 1**.

Table 1. Properties of the zeolites employed in this work.

Zeolite	**Particle size (μm)** [a]	**Density (g/cm^3)**	**Pore volume (cm^3/g)**	**Pore size** (Å)	**Si/Al**	**Reference**
CHA	1.0	1.508	0.33	3.8	5	[35-37]
LTA5	0.5	1.498	0.27	4	5	[37-41]
Rho	1.5	1.442	0.26	3.6	5	[33,42]

[a]: Observed by SEM, except Rho, which forms agglomerates with PTMSP as binder, so the particle size is taken from [33].

The gases used in the experiments were carbon dioxide (99.97 %), oxygen (>99.999 %) and nitrogen (>99.999 %) provided by Air Liquide (Spain).

The membrane thickness was analyzed by means of a digital micrometer (Mitutoyo digimatic micrometer, IP 65) with a high accuracy up to 0.001 mm. The average thickness of the membranes is 72.75 ± 5.46 μm, not being influenced by the type of zeolite, and not far from the nominal thickness of 100 μm expected. As all the membranes have similar thickness, the permeability values are not affected by this parameter. The density of same membranes was also determined after the permeation tests, to study gravimetrically the integrity or possible physical aging of the membrane. The nominal filler loading used were 5, 10 and 20 wt. % referred to PTMSP polymer ratio.

2.2 Characterization

Thermogravimetric analysis have been performed to determine the thermal degradation of the MMM using a DTG-60H thermobalance (Shimadzu, Japan) in air atmosphere at a heating rate of 10 K min^{-1} up to 973 K. The sample temperature was measured with an accuracy of ± 0.1 K and the TG sensitivity was about 1 µg.

The cross-sectional areas and the morphology of selected membranes of each composition were observed by scanning electron microscopy (SEM), using a Jeol JSM 5410 equipment, located at the Universidad Politécnica de Valencia. Membrane samples were fractured in liquid nitrogen, to obtain a clean cross section that is coated with gold to reduce the charging effects on the polymer surface.

The X-ray diffraction (XRD) of zeolite crystals and MMM was measured at the Servicio de Difracción de Rayos X y Análisis por Fluorescencia del Servicio General de Apoyo a la Investigación de la Universidad de Zaragoza. Data were collected at room temperature using a Rigaku/D/max 2500 diffractometer, provided with rotating anode, at 40 kV and 80 mA Cu Kα radiation with λ = 1.5418 Å and graphite monochromator.

Single gas permeability of N_2 and CO_2 was determined within the temperature range 298 – 333 K in a constant volume system experimental setup shown in **Figure 1**. The membrane module consists of two stainless pieces with a cavity where the membrane is placed on a 316LSS macroporous disk support of 20 µm nominal pore size (Mott Corp., USA) and sealed by Viton rings. The effective membrane area was 15.55 cm^2. In a typical run, the air tightness of the system was check before each permeation test, being tested, firstly, N_2 permeation tests and secondly, those with CO_2. The pure gas is fed at 2–3 bar into both permeate and feed compartments and then the permeate side is evacuated to generate the pressure difference across the membrane. Two transducers (Omega, UK)

measured the pressure in the feed side and across the membrane during the whole experiment, in order to monitor the gas volume that passes through it. Each permeation test takes, approximately 2 hours, for each temperature, and experimental runs under the same membrane compositions and separation conditions are repeated 3 times for reproducibility assessment. The accumulated permeate volume calculated from the registered pressures is plotted versus time in **Figure 2.**

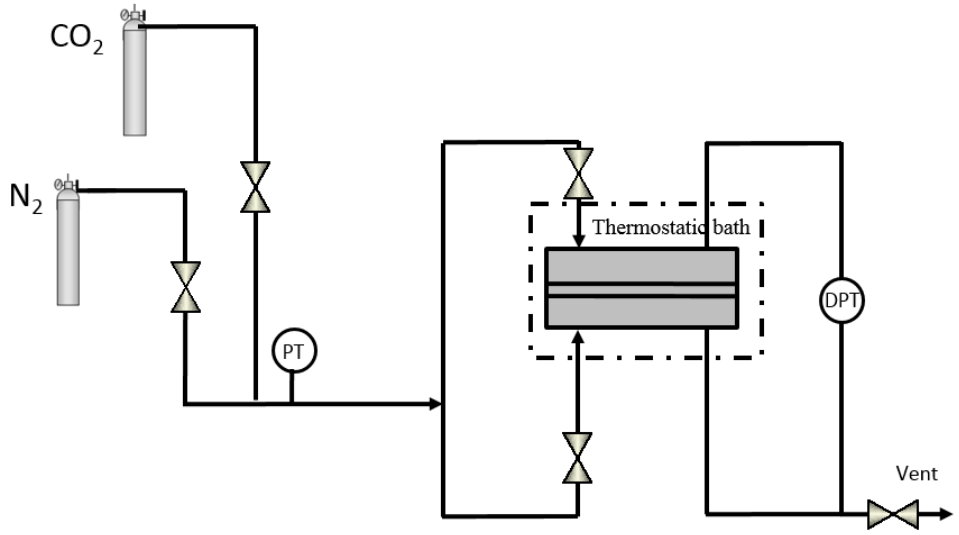

Figure 1. Experimental setup for the single gas permeation experiments.

When steady state was attained, the following expression was used to calculate the pure gas permeability, from the slope of the linear representation of the equation (1) [43], in a measurement interval around 1000 and 3000 s for CO_2 and N_2 permeability experiments, respectively, as

$$ln\left|\frac{\left(p_{i,f}-p_{i,p}\right)_0}{\left(p_{i,f}-p_{i,p}\right)}\right| = ln\left|\frac{\Delta p_0}{\Delta p}\right| = \left(\frac{P_i}{\delta}\right)\beta_m t \qquad (1)$$

where $p_{i,f}$ and $p_{i,p}$ are the feed and permeate partial pressures of the gas *i*, respectively, P_i is the permeability, δ is the thickness of the membrane and β_m is a geometric factor with a value of 110.76 m^{-1} in the experimental set up used in this work.

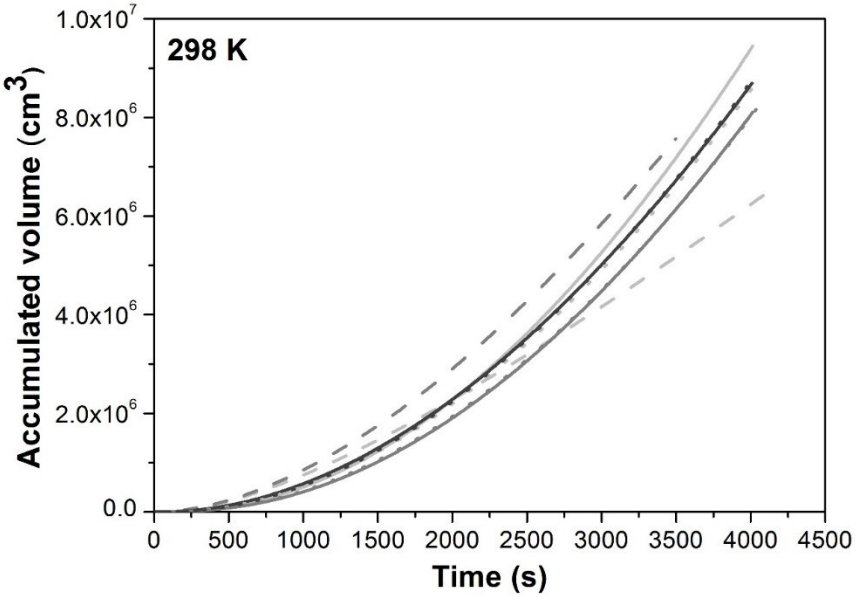

Figure 2. Accumulated volume versus time at 298 K for CO_2 permeation across the MMM. Continuous lines for LTA5-PTMSP, dashed lines for CHA-PTMSP membranes, and dotted lines for Rho-PTMSP membranes. 5 wt % (light gray), 10 wt % (gray), 20 wt % (black).

The transition regime of mass transfer through a dense material in Figure 2 allows us to estimate the diffusivity through the membranes according to

$$D = \delta^2 / 6\theta \qquad (1)$$

where δ is the membrane thickness and θ is the time-lag obtained extrapolating to the time axis the linear part of the experimental curve of the accumulated permeate volume vs.

time plot. Estimated time lag times range from 231 to 2103 s for CO_2 and N_2 permeation, respectively, for the membranes tested in this work.

The permeability is a function of the absolute temperature and it is described in an Arrhenius form equation (2) [44]

$$P = P_0 \, exp\left(-E_P / RT\right) \tag{2}$$

where P_0 is the pre exponential factor and E_p the activation energy of permeation.

The gas diffusivity also follows the Arrhenius model [44]

$$D = D_0 \, exp\left(-E_D / RT\right) \tag{3}$$

where D_0 is the pre exponential factor and E_D the activation energy of diffusion.

From the ratio of the single gas permeabilities of the most permeating gas, *i*, to the least permeating gas, *j*, the ideal selectivity can be calculated, as

$$\alpha = \frac{P_i}{P_j} \tag{4}$$

Gas separation experiments are carried out on selected membranes by means of CO_2/N_2 mixed gas separation tests using another experimental setup, schematized on **Figure 3**. The membrane module was the same as in the single gas permeation experiments. The feed mixture was set up at 12.5 wt. % CO_2/ 87.5 wt.% N_2 using MC-50SCCM-D mass flow controllers (Alicat Scientific, USA). This mixture is fed to the membrane module with temperature controlled by a Memmert UNE 200 convection oven. The permeate flow rate was measured at the exit using a flowmeter and the CO_2 concentration was measured at the end by a G100 analyser provided with a temperature probe (Fonotest, USA). The permeate is mixed with pure known N_2 flow rate for dilution, before entering the analyzer, since the maximum CO_2 concentration measured by the

analyser is 20%. The permeability, P_i, is calculated by equation (5) and the separation factor by equation (6).

$$P_i = \frac{Q_i \delta}{A \Delta p_i} \tag{5}$$

$$S.F. = \frac{y_{CO_2} / y_{N_2}}{x_{CO_2} / x_{N_2}} \tag{6}$$

where P_i is given in Barrer (1 Barrer = 10^{-10} cm^3 (STP)·cm/cm^2 s cmHg), i represents the penetrating gas i, Δp_i is the partial pressure difference of i across the membrane (cmHg), Q_i is the permeate flow rate of $_i$ (cm^3/s) at standard pressure and temperature and y and x are the concentration at the permeate and feed stream, respectively.

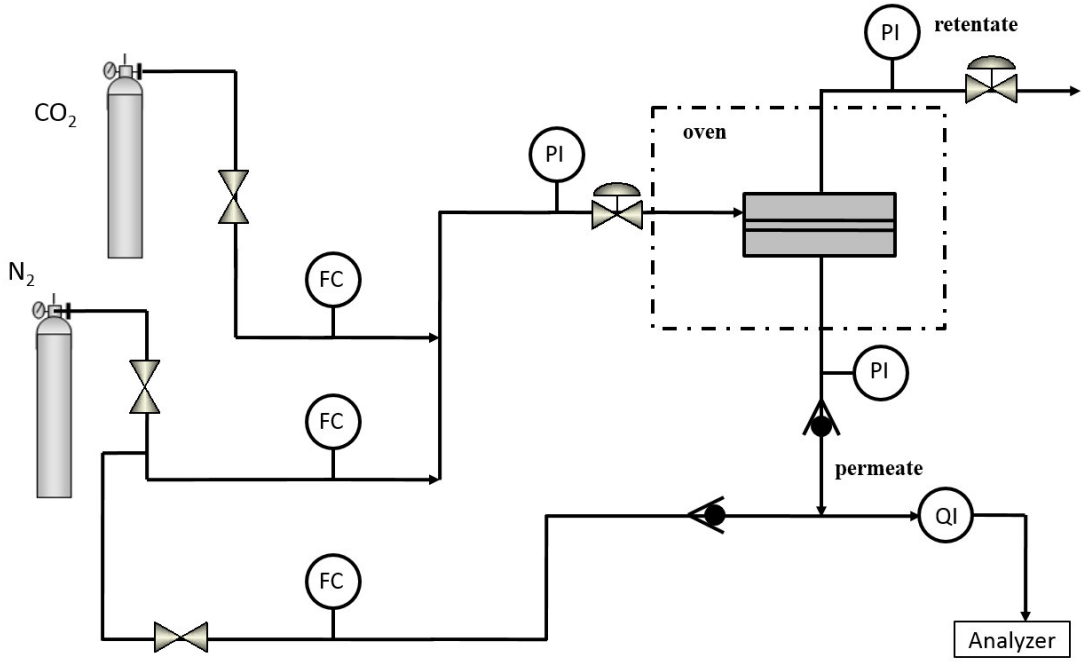

Figure 3. Experimental setup for the gas separation experiments.

3. Results and discussion

3.1. Synthesis and characterization

Before analyzing the influence of temperature on permeation, the thermal stability of the membranes was measured by Thermo Gravimetric Analysis (TGA). The TGA analyses of the MMM are presented in **Figure 4**. In can be observed that the decomposition of the pure PTMSP agrees with literature [45] and the thermal stability of the MMM is very similar to that of pure PTMSP, resisting temperatures up to 573 K.

From the thermogravimetric curves, the real filler composition has been calculated from the residual weight in TGA analyses, being 7.58 ± 3.30, 12.26 ± 3.26 and 20.35 ± 3.25 wt. % for 5, 10 and 20 wt. % CHA -PTMSP MMMs, respectively. In the case of LTA5-PTMSP MMM, the real zeolite loading is 8.48 ± 3.55, 10.48 ± 1.69 and 22.09 ± 2.09 wt. % for 5, 10 and 20 wt. %, respectively. For Rho-PTMSP MMM, the real zeolite loading is 7.65 ± 2.72, 10.30 ± 2.14 and 19.71 ± 2.90 for, 5, 10 and 20 wt. %, respectively. There is a lower deviation from the nominal values than those obtained for pure silica ITQ-29 [30], which points out to a good dispersion and adhesion of the particles with Si/Al of 5 in the membrane matrix. These results point out that these materials are thermally stable up to 573K, being potential materials to be used at industrial level where processes at elevated temperatures are carried out. Besides, from these thermogravimetric analysis, it can be observed that the nominal loading of the fillers agrees with real values.

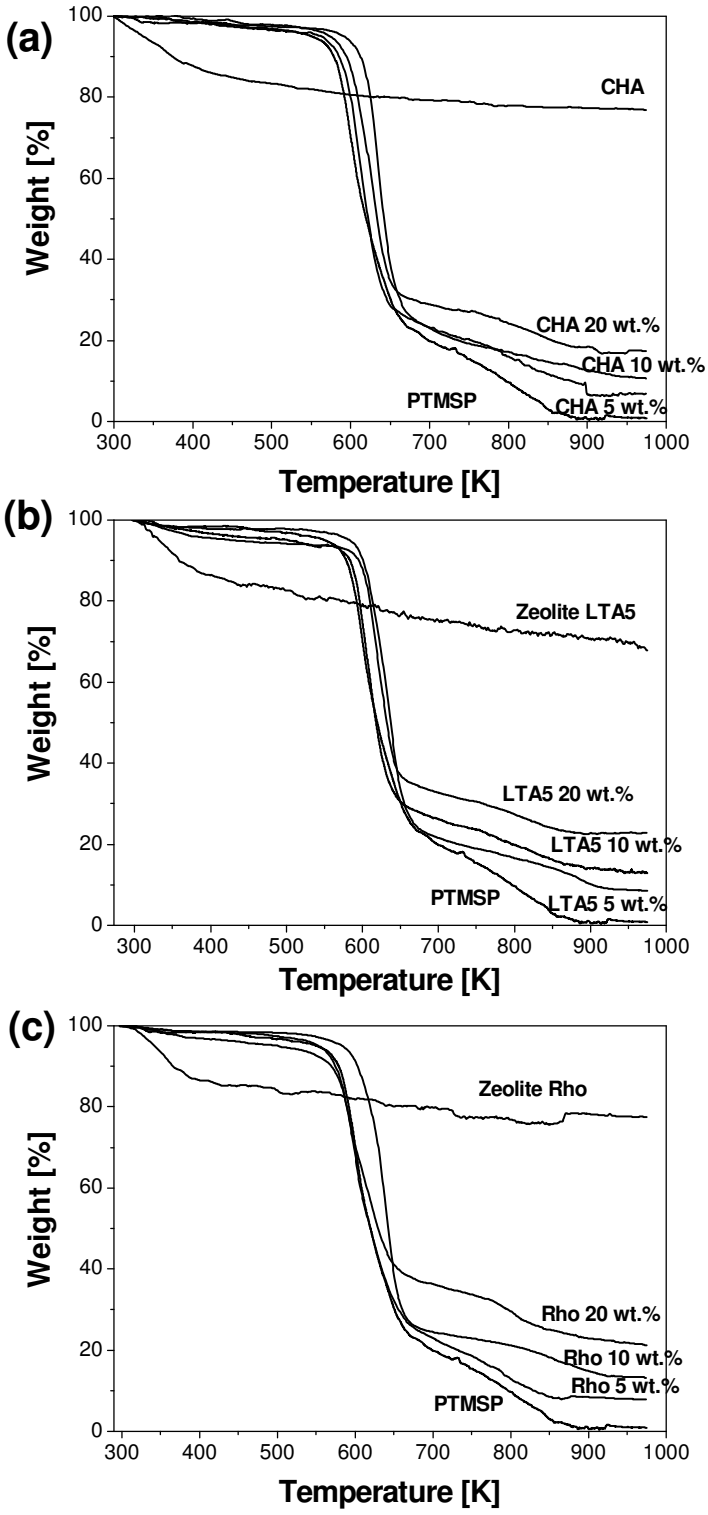

Figure 4. TGA of CHA-PTMSP (a) LTA5-PTMSP (b) and Rho-PTMSP (c) MMM.

The XRD patterns of the PTMSP-based MMM are shown in **Figure 5**. The main high intensity peaks of CHA are presented at diffraction angles of around 9º, 13º, 21º and 31º [46]. The characteristic reflections of CHA become stronger with the zeolite loading. The XRD also reveals the presence of this zeolite in the membrane matrix, because the peaks appear in the corresponding angles of CHA. In general, the narrower a high-intensity peak is, the more crystalline nature presents. The width of the peaks at 20 wt. % CHA is larger, probably, due to the appearance of voids at high loading that prevented obtaining reproducible permeation experiments [29]. This agrees with the XRD patterns of LTA-based MMMs drawn in **Figure 5 (b)**, where the high loading of 20 wt. % led to a dual layer structure as in LTA Si/Al = 1 in our previous work [29] and ZIF-8 in ZIF-8/PEBAX-5233 MMMs [47]. The XRD of LTA5-PTMSP and Rho-PTMSP membranes also reveal the presence of these zeolites in the membrane matrix, because the peaks appear in the corresponding angles of the LTA5 and Rho, respectively. Besides, as in Rho-PTMSP MMMs, the characteristic reflections of LTA5 and Rho zeolites become stronger with the filler loading.

Another observation that can be withdrawn from the XRD patterns in **Figure 5** is that the primary crystalline pattern of PTMSP is disrupted by the introduction of the zeolite particles, regardless the type of zeolite. The main broad band of PTMSP decreases with respect to increasing zeolite loading for all the types of zeolite under study. This means that the crystallinity of MMM has been modified upon addition of the zeolite particles, as observed before for similar systems [48].

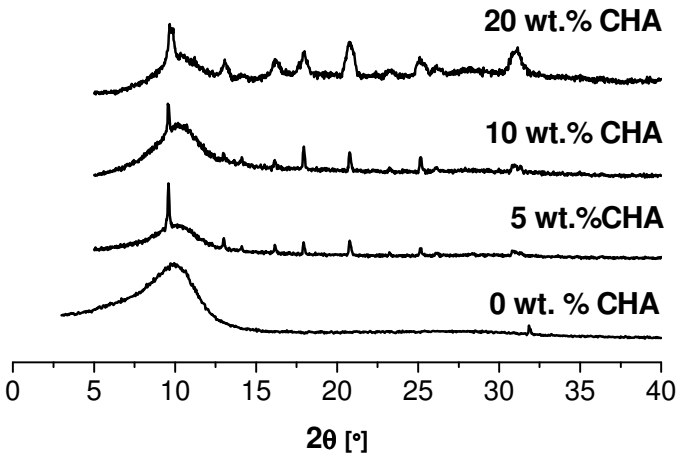
20 wt.% CHA
10 wt.% CHA
5 wt.%CHA
0 wt. % CHA
0
5
10
15
20
25
30
35
40
2θ [°]

(a)

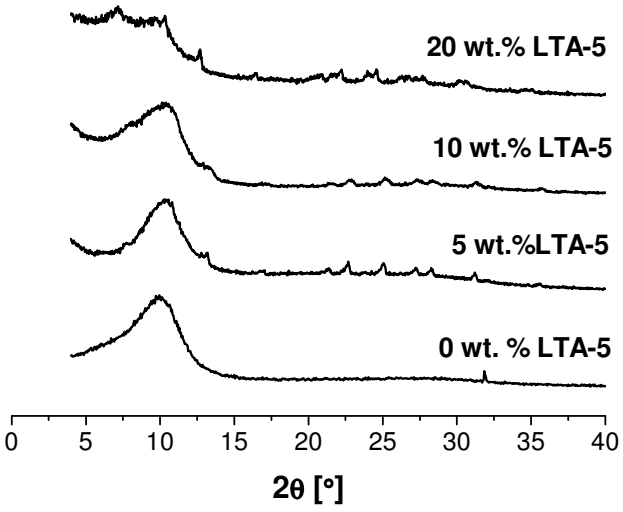
20 wt.% LTA-5
10 wt.% LTA-5
5 wt.%LTA-5
0 wt. % LTA-5
0
5
10
15
20
25
30
35
40
2θ [°]

(b)

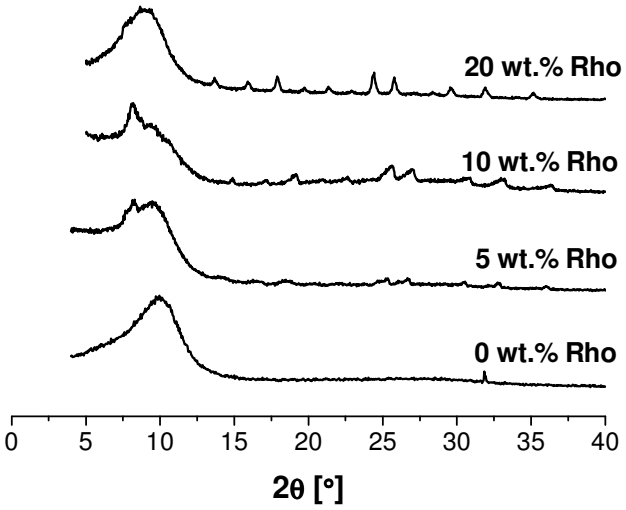

(c)

Figure 5. X-ray diffractogram of the (a) CHA, (b) LTA5 and (c) Rho-filled MMM.

The cross-section images of the MMM are shown in **Figure 6**. A heterogeneous distribution of the zeolites is shown due to their sedimentation on the membrane side in contact with the plate, leading to an asymmetric morphology in the membranes [25, 38]. In CHA-PTMSP and Rho-PTMSP MMM, the zeolite particles have a higher density (CHA 1.508 g cm^{-3}, Rho 1.442 g cm^{-3}) than the pure polymer (0.75 g cm^{-3}), and they accumulate at the bottom of the membrane. Better filler dispersion is observed for the LTA5-PTMSP membranes, which can be attributed to the smaller size of the LTA5 zeolite particles, and the tendency of Rho particles to form clusters of agglomerates at the bottom of the membrane. CHA particles are too large and dense to make defect-free 20 wt.% CHA-PTMSP MMMs.

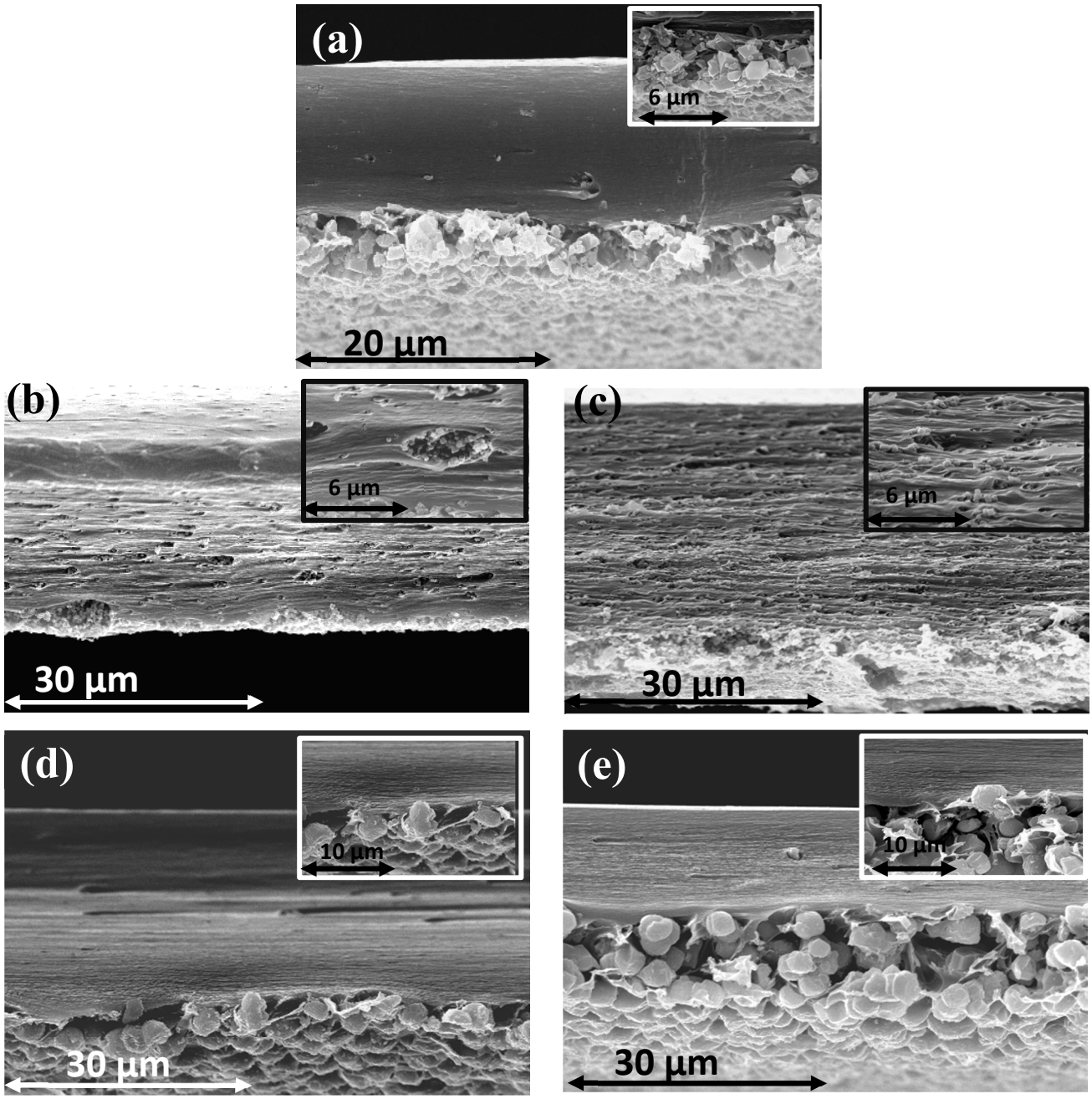

Figure 6. Cross-sectional images of the MMMs: (a) 5 wt. % CHA-PTMSP, (b) 5 wt. % LTA5-PTMSP, (c) 20 wt. % LTA5-PTMSP, (d) 5 wt.% Rho-PTMSP, (e) 20 wt. % Rho-PTMSP.

Zeolite with smaller particle sizes have lower effect at lower filler loadings on the membrane compaction. These compaction values have been calculated as the difference

between the membrane density before and after the set of permeation experiments. Each membrane is exposed to ten permeation experiments of two hours each, under an average pressure difference of 2.5 bar and in the consecutive temperature range from 298 to 333 K. These compaction values are collected in **Table 2**. This allows expecting higher resistance to physical aging, because of the free volume structure is kept for longer times [49].

Table 2. Compaction values of the MMM in increasing order of particle size: LTA, CHA, Rho.

	Density before experiment (g/cm^3)	**Density after experiment (g/cm^3)**	**Compaction**
5wt% LTA5-PTMSP	0.745 ± 0.02	0.566 ± 0.17	0.180 ± 0.08
10wt% LTA5-PTMSP	0.969 ± 0.25	0.785 ± 0.18	0.184 ± 0.03
20wt% LTA5-PTMSP	0.961 ± 0.35	0.861 ± 0.26	0.1 ± 0.10
5wt% CHA-PTMSP	0.771 ± 0.27	0.571 ± 0.08	0.2 ± 0.06
10wt% CHA-PTMSP	0.896 ± 0.08	0.739 ± 0.05	0.154 ± 0.03
5wt% Rho-PTMSP	0.899 ± 0.13	0.688 ± 0.07	0.211 ± 0.06
10wt% Rho-PTMSP	0.638 ± 0.11	0.517 ± 0.12	0.122 ± 0.08
20wt% Rho-PTMSP	1.051 ± 0.28	0.900 ± 0.10	0.152 ± 0.07

3.2 Influence of temperature on transport properties

The former observations can be related to the permeability, diffusivity and selectivity of the MMM in comparison with the pure PTMSP membrane. The gas permeability through the pure PTMSP membranes prepared in our laboratory decreases with increasing temperature, from 17454 ± 5102 Barrer at 298 K to 12056 ± 2375 Barrer

at 333 K, whereas the ideal CO_2/N_2 selectivity is not improved. This is a typical behavior for PTMSP, due to the high free volume, and the fact that the rigid and weakly molecular sieving structure is more prone to changes in solubility than diffusivity [12, 13].

Contrarily, the CO_2 permeability of the MMM prepared in this work generally increases with temperature, for each zeolite loading and zeolite type. The average deviations errors for gas permeability measured are 7, 10 and 15 % for Rho, LTA5 and CHA-PTMSP based MMM, respectively The CO_2/N_2 ideal selectivity of the MMM is higher than that of the pure PTMSP, in the temperature range under study. The CO_2/N_2 selectivity of 5 wt. % Rho-PTMSP MMM increases from 6.19 to 13.54, CHA-PTMSP MMM from 7.78 to 31.6, and LTA5-PTMSP MMM from 9.00 to 27.88, when increasing the temperature from 298 to 333 K. This is why the Robeson's upper bound for CO_2/N_2 separation, in **Figure 7** is overcome for the intermediate loading MMM when increasing the temperature from 298 to 323 K. In **Figure 7**, the permselectivity values of the pure PTMSP membranes, prepared in this work in a similar manner as the MMM, are included, for the sake of comparison. The upper bound trade off relationship between permeability and selectivity has been calculated as function of temperature, taking into account the parameters obtained by Rowe et al. [50]. The upper bound shifts vertically with temperature and in the case of the CO_2/N_2 separation moves downwards with an increase in temperature [50]. Therefore, the permselectivity of the MMM is improved up to 280 % and 2800 % higher at 298 and 323 K, respectively, compared to that of the pure PTMSP membranes.

Another observation from the experimental single gas permeation of the MMM studied in this work is that the effect of the temperature on the CO_2 permeability varies with the zeolite loading and morphology. Although the CO_2 permeability decreases with zeolite filler content regardless the type of filler, the selectivity of LTA5, CHA and Rho-

PTMSP MMM reaches values of 9.27, 15.93 and 6.19 at 298 K, respectively, much higher than that of the pure PTMSP membranes (α (CO_2/N_2) =1.22 ± 0.07) at the same temperature measured in the permeation setup in **Figure 1**. This occurs at 10 wt. % loading for the smallest particle size zeolites (LTA5 and CHA) and 5 wt. % for the largest Rho particles, which is in agreement with the XRD and SEM observations. The CO_2 permeability, of some MMM at certain content of zeolite loading and temperature, is not decreased, though, contrarily to the general permselectivity trade-off reported for MMM. For instance, for 5 wt. CHA-based MMM at 333K, the CO_2 permeability is not decreased, while for LTA5 and Rho –based MMM at 303 and 323K, respectively, the CO_2 permeability is almost constant up to a loading of 10 wt. %. This is because of polymer chain rigidification around the zeolite particles, partial pore blockage of zeolites by the polymer chains and extended diffusion pathways of the penetrants through the membrane [51-55], with constant or decreasing selectivity [23]. This behavior is attributed to the molecular sieving effect imparted by the introduction of the small-pore zeolites in the membrane, as well as the good interaction with the PTMSP chains that prevents interfacial voids. In general, CO_2/N_2 selectivity increases only up to 10 wt. % zeolite content, decreasing again when the zeolite loading is raised to 20 wt.%, due to the appearance of voids. The agglomeration of excess particles at the bottom observed by SEM **(Figure 6)** generate the preferential orientations observed by XRD (**Figure 5**) that lead to poorer adhesion between some particles and the polymer, providing that obtaining a good adhesion is especially difficult when using glassy polymers with rigid structure [27]. Moore and Koros established in 40 wt. % the upper limit over which a zeolite 4A could not be added to a glassy polymer without generating defects that decrease the selectivity gained [56]. In this work, the CO_2/N_2 selectivity is considerably increased even at zeolite loadings as low as 5 and 10 wt. %, improving the CO_2 permselectivity.

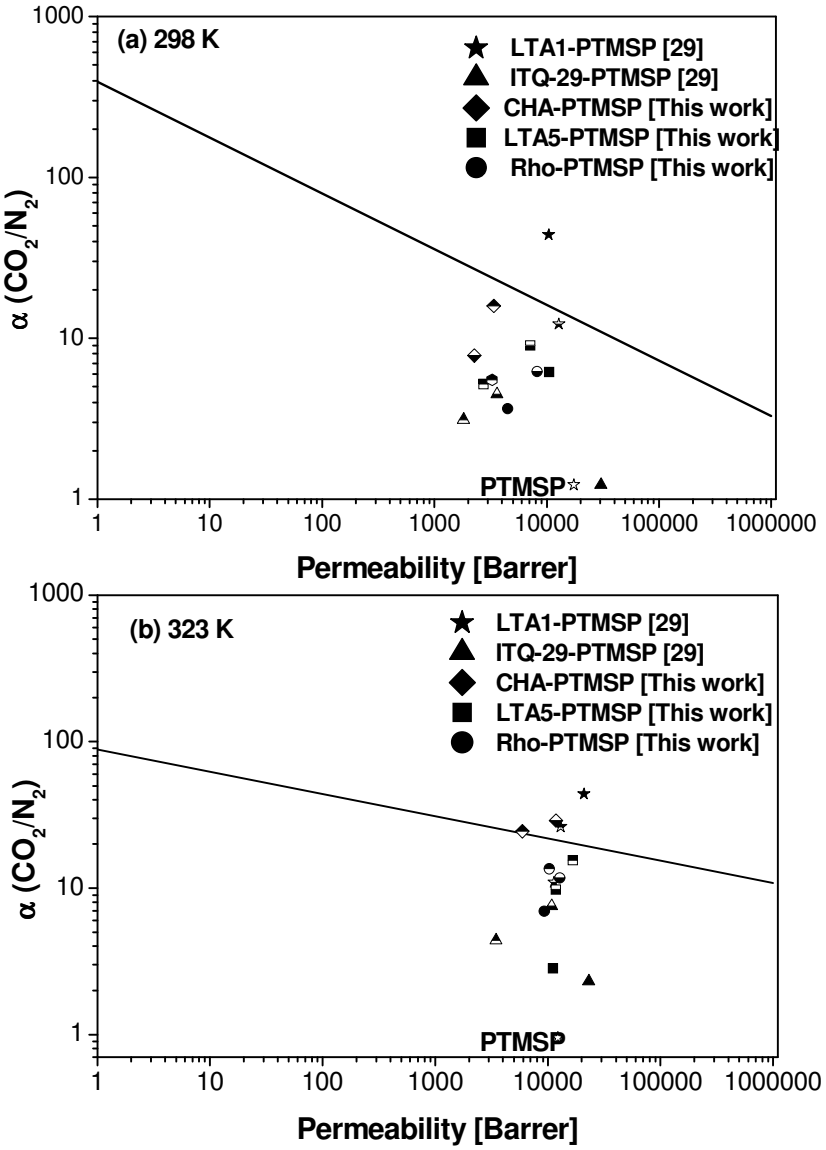

Figure 7. Comparison of the permselectivity of the MMM prepared in this work at 298 K (a) and 323 K (b), in comparison with the Robeson's upper bound for CO_2/N_2 gas pair separation [9, 50]. Half symbols represent 5 wt. % (▄) and 10 wt. % (▀) loadings, respectively, and full symbols, 20 wt. %.

The permselectivity of the LTA5, Rho and CHA-PTMSP MMM prepared in this work is enhanced with increasing operation temperature from 298 K to 333 K. Indeed, at 323 K, Robeson's upper bound is surpassed by 5 and 10 wt. % CHA -PTMSP and 10 wt.

% LTA-PTMSP MMM, while the data obtained for 5 wt. % LTA5-PTMSP and Rho-PTMSP MMMs are almost on the Robeson's upper bound limit. In conclusion, selectivity is much greater than that of pure PTMSP membranes, due to the molecular sieving effect of the incorporation of the small-pore zeolites to the polymer matrix and the absence of defects between the polymer and the zeolites in the membrane matrix. Moreover, permeabilities are not substantially reduced compared to the pure polymer and all this results on overcoming the existing polymer membranes performance [57-60].

The effect of filler type and filler content on the CO_2 permeability is represented at 298 and 323 K, in **Figure 8 (a)** and **8 (b)**, respectively. The relative CO_2 permeability of the MMM with respect to that of the pure PTMSP membranes is plotted versus zeolite loading for the three different morphologies. At 298 K, the CO_2 permeability of both CHA and LTA5 PTMSP based MMM is enhanced with the filler content, while the best CO_2 permeability of Rho-PTMSP MMM at 298 K is obtained at a zeolite loading of 10 wt%. On the other hand, at 323 K the CO_2 permeability of CHA and Rho PTMSP MMM decreases with zeolite loading, while the highest CO_2 permeability through LTA5-PTMSP MMM is obtained for a filler content of 10 wt. %, being higher than that of pure PTMSP membranes measured in the same conditions. At both temperatures the lowest decrease of CO_2 permeability with increasing zeolite loading are obtained for the LTA5-PTMSP MMM.

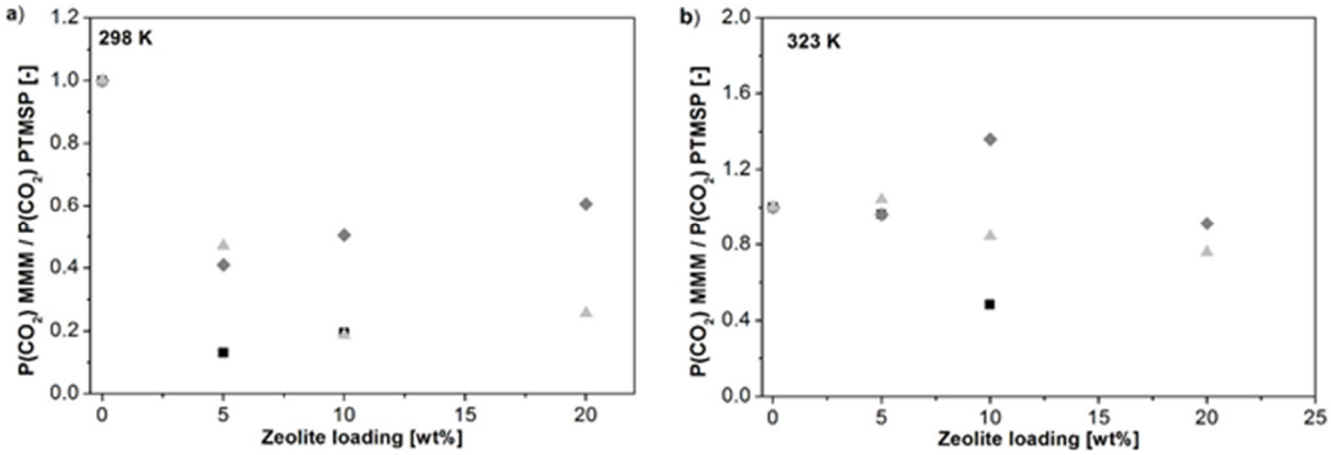

Figure 8. Relative CO_2 permeability of the different MMM with respect to that of pure PTMSP membranes versus zeolite content at 298 K **a)** and 323 K **b).** CHA- (black), LTA5- (gray) and Rho- (light gray) based PTMSP MMM.

The effect of filler type and filler content on the CO_2/N_2 selectivity at 298 and 323 K has been also presented **(Figure 9 a) and 9 b)).** The relative CO_2/N_2 selectivity to that of the pure PTMSP membranes is plotted as a function of zeolite loading and morphology. At 298 K, both the CO_2/N_2 selectivity of Rho and LTA- PTMSP based MMM decrease with filler content, being the highest with a 5 wt% zeolite loading, while the CO_2/N_2 selectivity of CHA-PTMSP MMM enhances with an increase in the filling. On the contrary, at 303 K the best CO_2/N_2 selectivity of CHA-PTMSP MMM is with a filler content of 5 wt%, while that of LTA and Rho-PTMSP based MMM increases up to a zeolite loading of 10 wt%, decreasing again when the filler charge is raised to 20 wt. %, probably due to the appearance of voids. However, the CO_2/N_2 selectivity is considerably enhanced compared to that of the pure PTMSP membranes, up to a factor of 30.

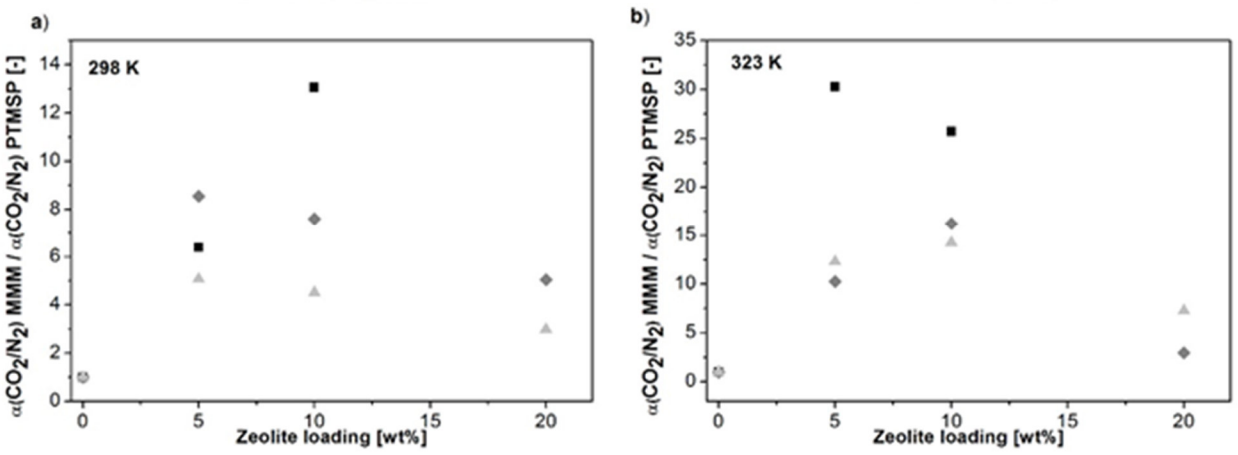

Figure 9. Relative CO_2/N_2 selectivity of the different MMM with respect to that of pure PTMSP membranes versus zeolite content at 298 K **a)** and 323 K **b).** CHA- (black), LTA5- (gray) and Rho- (light gray) based PTMSP MMM.

The permeation tests carried out at different temperatures agreed with Arrhenius-type relationships, according to equation (3) and (4) (not shown). Noteworthy, LTA5-PTMSP MMM give the highest permeabilities, probably because LTA5 zeolite has the largest pore size. This enhances the diffusivity contribution to permeation of LTA5-based MMM, compared with the others, because of the 3-dimensionally interconnected larger pores of the LTA5 zeolite particles [61]. The activation energies for permeation are –7.1 ± 1.4 and –12.6 ± 4.1 kJ mol^{-1} for CO_2 and N_2 through pure PTMSP membranes, respectively, which agrees with other authors [58]. While the energies for diffusion are -7.12 ± 4.99 and -17.29 ± 8.34 kJ mol^{-1} for CO_2 and N_2, respectively, also in agreement with other works [12, 48]. The activation energies for permeation and diffusion through the MMMs are presented in **Table 3**. The higher the temperature effect on the diffusion rate, the higher is the energy activation for diffusion and the higher the influence of diffusivity of permeation [48]. In this work, the MMMs present positive values for the activation energy for permeation that are greater than that of the pure polymer, because

the solubility of the Si/Al = 5 zeolites used as fillers is also playing a role. From **Table 3,** it is evident that the positive value of E_p in the membrane is accompanied by a positive value of E_D, only when the MMM start forming a dual phase structure and thus behaving like a pure inorganic membrane. A negative E_p value is accompanied also by a negative value of E_D for the better dispersed LTA5-PTMSP MMM at zeolite loadings of 5 and 10 wt.%, of lower particle size than CHA and Rho.

Table 3. Activation energies of permeation and diffusion for CO_2 and N_2 through the PTMSP-based MMM.

Membrane	**wt.% loading**	**E_p [kJ/mol]**		**E_D [kJ/mol]**	
		CO_2	**N_2**	**CO_2**	**N_2**
PTMSP	0	-7.10 ± 1.4	-12.6 ± 4.1	-7.12 ± 4.99	-17.29 ± 8.34
CHA-PTMSP	5	46.53 ± 14.72	12.13 ± 3.17	25.15 ± 8.89	12.85 ± 2.28
	10	16.53 ± 8.75	7.19 ± 2.67	25.15 ± 9.47	1.36 ± 0.30
LTA 5-PTMSP	5	-11.23 ± 9.18	42.29 ± 13.05	-4.56 ± 2.61	28.25 ± 1.65
	10	18.76 ± 16.18	42.46 ± 15.17	21.18 ± 3.35	21.25 ± 2.92
	20	-5.88 ± 1.38	23.14 ± 16.14	-10.05 ± 1.54	43.96 ± 15.27
Rho-PTMSP	5	14.64 ± 3.68	-5.04 ± 0.69	15.50 ± 7.23	-12.35 ± 8.15
	10	26.43 ± 2.75	21.38 ± 8.54	22.94 ± 0.27	13.63 ± 3.21
	20	18.33 ± 4.51	10.14 ± 3.21	2.89 ± 0.67	13.04 ± 4.62

3.3 Mixed gas separation properties

Once the novel MMM were characterized, the MMM showing the highest separation ability of all studied in this work were those loaded with 5 wt. % regardless the type of zeolite. The separation of CO_2/N_2 gas mixtures at 12.5% CO_2 was measured at 333 K and 4 bar, which approaches real mixed gas separation in flue gas post combustion treatment. Results are collected in **Table 4**. The permeation was calculated from the mixed gas separation set-up in **Figure 3**, by equation (7). Both CO_2 permeation and ideal selectivity of LTA5 and Rho-filled MMM were enhanced in mixed gas separation in comparison with single gas permeation experiments, whereas this was not observed when CHA was used as filler. The real separation factor was calculated using equation (8). The separation factor has lower values than the ideal selectivity, because the zeolites and MMM adsorb preferentially the CO_2 thus hindering the largest N_2 molecule diffusion through the membrane. This implies a final CO_2 percentage in the permeate of 46.8 %, 43.4 % and 42.0 % and in the retentate 9.52 %, 9.06 % and 8.47 % for CHA-PTMSP, LTA5-PTMSP and Rho-PTMSP, respectively. The CO_2 permeabilities are also enhanced as compared with the single gas permeation experiments, which proves the influence of diffusivity selectivity despite the preferential sorption for CO_2 over N_2 of both zeolites and MMM, as in other membrane systems [62].

Table 4. CO_2/N_2 separation of 5 wt. % loaded MMMs at 333 K and 12.5% CO_2 in the feed mixture.

Zeolite filler	**P(CO_2) [Barrer]**	**P(N_2) [Barrer]**	**Ideal Selectivity, α**	**% CO_2 in permeate**	**Separation factor (S.F.)**
CHA	22914	692	33.13	46.8	6.2
LTA5	27249	1242	21.94	43.4	5.4
Rho	64920	1308	49.65	42.0	5.1
Zeolite A *	112627	1785	63.10	39.6	4.9

*This experiment was carried out with the 20 wt. % loaded zeolite A in PTMSP, whose characterization was studied in a previous work [29].

4. Conclusions

In this work, mixed matrix membranes (MMM) have been successfully prepared using the highly permeable PTMSP polymer and small-pore zeolites with Si/Al ratio of 5, and topologies LTA5, CHA and Rho, respectively, by the solution casting method. A filler loading of 5 and 10 wt. % in the PTMSP matrix provides good thermal stability as well as adhesion and dispersion throughout the MMM. The permselectivity of N_2 and CO_2, increased with the incorporation of all the zeolites. The CO_2 permeability through the membrane decreases, but the CO_2/N_2 selectivity is considerably improved, in consequence enhancing the CO_2 permselectivity. The adhesion at the highest filler loading of 20 wt. % is hindered by agglomeration and irregular particle orientation that causes voids appearance between the phases, as observed by XRD and SEM.

The increase in CO_2/N_2 permselectivity over the Robeson's upper bound for this gas pair mixture is enhanced when operation temperature is increased from 298 K to 333 K. This is attributed to the molecular sieving effect upon zeolite introduction, which was

maintained even at increasing temperature. In fact, at 323 K not only LTA-PTMSP membrane but also CHA-PTMSP membranes surpass this upper bound.

The 5 wt. % zeolite MMM performance were tested for the CO_2/N_2 mixture separation at 333 K. Mixed gas separation experiments reveal similar CO_2 permeability and higher CO_2/N_2 ideal selectivity as in single gas permeation, and low real separation factor, thus proving the higher influence of diffusivity selectivity despite the preferential sorption for CO_2 over N_2 of both zeolites and MMM.

These results indicate the good compatibility between the Si/Al = 5 zeolite fillers and the PTMSP to produce novel membrane materials with improved permselectivity and the potential of these membranes to be used in CO_2 separation at higher temperature than conventional processes.

Acknowledgements

Financial support from the Spanish Ministry of Economy and Competitiveness (MINECO) under project CTQ2012-31229 at the Universidad de Cantabria and MAT2012-38567-C02-01 and Severo Ochoa SEV-2012-0267 at the ITQ (UPV-CSIC) are gratefully acknowledged. A.F.B. and C.C.C. also thank the MINECO for the Early Stage Researcher (BES2013-064266) and ‘‘Ramón y Cajal’’ tenure-track (RYC2011-0855) contracts, respectively.

References

[1] R.S. Haszeldine, Carbon capture and storage: how green can black be?, Science 325 (2009) 1647-1652.

[2] E. Favre, Carbon dioxide recovery from post-combustion processes: Can gas permeation membranes compete with absorption?, J. Membr. Sci., 294 (2007) 50-59.

[3] G.T. Rochelle, Amine scrubbing for CO_2 capture, Science, 325 (2009) 1652-1654.

[4] T.C. Merkel, H. Lin, X. Wei, R. Baker, Power plant post-combustion carbon dioxide capture: an opportunity for membranes, J. Membr. Sci., 359 (2010) 126-139.

[5] P. Luis, T.V. Gerven, B.V.d. Bruggen, Recent developments in membrane-based technologies for CO_2 capture, Prog. Energ. Comb. Sci., 38 (2013) 419-448.

[6] R. Bredesen, K. Jordal, O. Bolland, High-temperature membranes in power generation with CO_2 capture, Chem. Eng. Proc., 43 (2004) 1129-1158.

[7] B.T. Low, L. Zhao, T.C. Merkel, M. Weber, D. Stolten, A parametric study of the impact of membrane materials and process operating conditions on carbon capture from humidified flue gas, J. Membr. Sci., 431 (2013) 139-155.

[8] K. Ramasubramanian, H. Verweij, W.S.W. Ho, Membrane processes for carbon capture from coal-fired power plant flue gas: A modeling and cost study, J. Membr. Sci., 421-422 (2012) 299-310.

[9] L.M. Robeson, The upper bound revisited, J. Membr. Sci., 320 (2008) 390-400.

[10] M. Rezakazemi, A.E. Amooghin, M.M. Montazer-Rahmati, A.F. Ismail, T. Matsuura, State-of-the-art membrane based CO_2 separation using mixed matrix membranes (MMMs): An overview on current status and future directions, Prog. Pol. Sci., 39 (2014) 817-861.

[11] R. Mahajan, W.J. Koros, Factors controlling successful formation of mixed-matrix gas separation materials, Ind. Eng. Chem. Res., 39 (2000) 2692-2696.

[12] X.-Y. Wang, A.J. Hill, B.D. Freeman, I.C. Sanchez, Structural, sorption and transport characteristics of an ultrapermeable polymer, J. Membr. Sci., 314 (2008) 15-23.

[13] K. Nakamura, T. Kitagawa, S. Nara, T. Wakamatsu, Y. Ishiba, S. Kanehashi, S. Sato, K. Nagai, Permeability of Dry Gases and Those Dissolved in Water through Hydrophobic High Free-Volume Silicon- or Fluorine-Containing Nonporous Glassy Polymer Membranes, *Ind Eng. Chem. Res.* 52 (2013), 1133−1140.

[14] L. Starannikova, V. Khodzhaeva, Y. Yampolskii, Mechanism of aging of poly[1-(trimethylsilyl)-1-propyne] and its effect on gas permeability, J. Membr. Sci., 244 (2004) 183-191.

[15] A. Morisato, H.C. Shen, S.S. Sankar, B.D. Freeman, I. Pinnau, C.G. Casillas, Polymer characterization and gas permeability of poly(1-trimethylsilyl-1-propyne) [PTMSP], poly(1-phenyl-1-propyne) [PPP], poly(1-phenyl-1-propyne) [PPP], and PTMSP/PPP blends, J. Polym. Sci. B, 34 (1998) 2209-2222.

[16] K. Nagai, T. Masuda, T. Nakagawa, B.D. Freeman, I. Pinnau, Poly[1-(trimethylsilyl)-1-propyne] and related polymers: synthesis, properties and functions, Prog. Pol. Sci., 26 (2001) 721-798.

[17] C.E. Powell, G.G. Qiao, Polymeric CO_2/N_2 gas separation membranes for the capture of carbon dioxide from power plant flue gases, J. Membr. Sci., 279 (2006) 1-49.

[18] T.C. Merkel, B.D. Freeman, R.J. Spontak, Z. He, I. Pinnau, P. Meakin, A.J. Hill, Sorption, transport and structural evidence for enhanced free volume in poly(4-methyl-2-pentyne)/fumed silica nanocomposite membranes, Chem. Mater., 15 (2003) 109-123.

[19] W. Yave, K.-V. Peinemann, S. Shishatsky, V. Khotmiskiy, M. Chirkova, S. Matson, E. Litvinova, N. Lecerf, Synthesis, characterization and membrane properties of poly(1-trimethylgermyl-1-propyne) and its nanocomposite with TiO_2, Macromol., 40 (2007) 8991-8998.

[20] M. Woo, J. Choi, M. Tsapatsis, Poly(1-trimethylsilyl-1-propyne)/MFI composite membranes for butane separations, Micropor. Mesopor. Mat., 110 (2008) 330-338.

[21] J. Gascón, F. Kapteijn, B. Zornoza, V. Sebastián, C. Casado, J. Coronas, Practical approach to zeolitic membranes and coatings: State of the art, opportunities, barriers and future perspectives, Chem. Mater., 24 (2012) 2829-2844.

[22] C.I. Chaidou, G. Pantoleontos, D.E. Koutsonikolas, S.P. Kaldis, G.P. Sakellaropoulos, Gas separation properties of polyimide-zeolite mixed matrix membranes, Sep. Sci. Technol., 47 (2012) 950-962.

[23] H. Karkhanechi, H. Kazemian, H. Nazockdast, M.R. Mozdianfard, S.M. Bidoki, Fabrication of homogeneous polymer-zeolite nanocomposite as mixed-matrix membranes for gas separation, Chem. Eng. Technol., 35 (2012) 885-892.

[24] R. Mahajan, W.J. Koros, Mixed matrix membrane materials with glassy polymers. Part 1, Polym. Eng. Sci., 42 (2002) 1420-1431.

[25] D. Sen, H. Kalipcilar, L. Yilmaz, Development of polycarbonate based zeolite 4A filled mixed matrix gas separation membranes, J. Membr. Sci., 303 (2007) 194-2013.

[26] Y. Li, W.B. Krantz, T.-S. Chung, A novel primer to prevent nanoparticle agglomeration in mixed matrix membranes, AIChE J., 53 (2007) 2470-2475.

[27] R. Mahajan, R. Burns, M. Schaeffer, W.J. Koros, Challenges in forming successful mixed matrix membranes with rigid polymeric materials, J. Appl. Pol. Sci., 86 (2002) 881-890.

[28] J. Ahmad, M.B. Hägg, Effect of zeolite preheat treatment and membrane post heat treatment on the performance of polyvinyl acetate/zeolite 4A mixed matrix membrane, Sep. Purif. Technol., 115 (2013) 163-171.

[29] A. Fernández-Barquín, C. Casado-Coterillo, M. Palomino, S. Valencia, A. Irabien, LTA/poly(1-trimethylsilyl-1-propyne) mixed matrix membranes for high-temperature CO_2/N_2 separation, Chem. Eng. Technol., 38 (2015) 658-666.

[30] C. Casado-Coterillo, J. Soto, M.T. Jimaré, S. Valencia, A. Corma, C. Téllez, J. Coronas, Preparation and characterization of ITQ-29/polysulfone mixed-matrix membranes for gas separation: effect of zeolite composition and crystal size, Chem. Eng. Sci., 73 (2012) 116-122.

[31] N. Kosinov, C. Auffret, G.J. Borghuis, V.G.P. Sripathi, E.J.M. Hensen, Influence of Si/Al ratio on the separation properties of SSZ-13 zeolite membranes, J. Membr. Sci., 484 (2015) 140-145.

[32] E.J. García, J. Pérez-Pellitero, G.D. Pirngruber, C. Jallut, M. Palomino, F. Rey, S. Valencia, Tuning the adsorption properties of zeolites as adsorbents for CO_2 separations: best compromise between the working capacity and selectivity, Ind. Eng. Chem. Res., 53 (2014) 9860-9874.

[33] M. Palomino, A. Corma, J.L. Jordá, F. Rey, S. Valencia, Zeolite Rho: a highly selective adsorbent for CO_2/CH_4 separation induced by a structural phase modification, Chem. Comm., 48 (2012) 215-217.

[34] M.M. Lozinska, J.P.S. Mowat, P.A. Wright, S.P. Thompson, J.L. Jorda, M. Palomino, S. Valencia, F. Rey, Cation gating and relocation during the highly selective "trapdoor" adsorption of CO_2 on univalent cation forms of zeolite Rho, Chem. Mater., 26 (2014) 2052-2061.

[35] E. Kim, T. Lee, H. Kim, W.-J. Jung, D.-Y. Han, H. Baik, N. Choi, J. Choi, Chemical Vapor Deposition on Chabazite (CHA) zeolite membranes for effective post-combustion CO_2 capture, Environ. Sci. Technol., 48 (2014) 14828-14836.

[36] S. I. Zones, Conversion of Faujasites to High-silica Chabazite SSZ-13 in the Presence of N,N,N-Trimethyl-l -adamantammonium Iodide, J. Chem. Soc. Faraday Trans., 87 (1991), 3709-3716

[37] M.M. Lozinska, E. Mangano, J.P.S. Mowat, A.M. Shepherd, R.F. Howe, S.P. Thompson, J.E. Parker, S. Brandani, P.A. Wright, Understanding carbon dioxide adsorption on univalent cation forms of the flexible zeolite Rho at conditions relevant to carbon capture from flue gases, J. Am. Chem. Soc., 134 (2012) 17628-17642.

[38] G. Clarizia, C. Algieri, E.Drioli, Filler-polymer combination: a route to modify gas transport properties of a polymeric membrane, Polymer, 45 (2004) 5671-5681.

[39] A. García, S. Eceolaza, M. Iriarte, C. Uriarte, A. Etxeberria, Barrier character improvement of an amorphous polyamide (Trogamid) by the addition of a nanoclay, J. Membr. Sci., 301 (2007) 190-199.

[40] M. Palomino, A. Corma, F. Rey, S. Valencia, New insights on CO_2 - methane separation using LTA zeolites with different Si/Al ratios and a first comparison with MOFs, Langmuir, 26 (2009) 1910-1917.

[41] J. G. Moscoso, G. J. Lewis, J. L. Gisselquist, M. A. Miller, L. M. Rohde, UZM-16: a crystalline aluminosilicate zeolitic material. WO Patent 03/068679, (2003).

[42] T. Chatelain, J. Patarin, E. Fousson, M. Soulard, J. L. Guth and P. Schulz, Synthesis and characterization of high-silica zeolite RHO prepared in the presence of 18-crown-6 ether as organic template. Microporous Mater., 4, (1995) , 231-238.

[43] E.L. Cussler, Diffusion. Mass transfer in fluid systems, 3rd ed., Cambridge University Press, Cambridge, 2007.

[44] J. Crank, The mathematics of diffusion, 2nd ed., Clarendon Press, Oxford, 1975.

[45] M.L. Chua, L. Shao, B.T. Low, Youchang, T.-S. Chung, Polyetheramine-polyhedral oligomeric silsesquioxane organic-inorganic hybrid membranes for CO_2/H_2 and CO_2/N_2 separation, J. Membr. Sci., 385-386 (2011) 40-48.

[46] C. Baerlocher, L.B. McCusker, Database of Zeolite Structures: http://www.iza-structure-org/database/. (last accessed on 2015/06/29)

[47] V. Nafisi, M.-B. Hägg, Development of dual layer of ZIF-8/PEBAX-2533 mixed matrix membrane for CO_2 capture, J. Membr. Sci., 459 (2014) 244-255.

[48] J. Ahmad, M.-B. Hägg, Development of matrimid/zeolite 4A mixed matrix membrane using low boiling point solvent, Sep. Purif. Technol., 115 (2013) 190-197.

[49] D.F. Sanders, Z.P. Smith, R. Guo, L.M. Robeson, J.E. McGrath, D.R. Paul, B.D. Freeman, Energy-efficient polymeric gas separation membranes for a sustainable future: A review, Polymer, 54 (2013) 4729-4761.

[50] B.W. Rowe, L.M. Robeson, B.D. Freeman, D.R. Paul, Influence of temperature on the upper bound: Theoretical considerations and comparison with experimental results., J. Membr. Sci., 360 (2010) 58-69.

[51] J. Qiu, K.-V. Peinemann, Gas transport properties of novel mixed matrix membranes with the organic filler trimethylsilyl-glucose, Desal., 199 (2006) 113-114.

[52] M.G. Süer, N. Bac, L. Yilmaz, Gas permeation characteristics of polymer-zeolite mixed matrix membranes, J. Membr. Sci., 91 (1994) 77-86.

[53] T.T. Moore, W.J. Koros, Non-ideal effects in organic-inorganic materials for gas separation membranes, J. Mol. Struct., 739 (2005) 87-98.

[54] Y. Li, T.-S. Chung, C. Cao, S. Kulprathipanja, The effects of polymer chain rigidification, zeolite pore size and pore blockage on polyether sulfone (PES)-zeolite A mixed matrix membranes, J. Membr. Sci., 260 (2005) 45-55.

[55] Z. Huang, Y. Li, R. Wen, M.M. Teoh, S. Kulprathipanja, Enhanced gas separation properties by using nanostructured PES-zeolite 4 A mixed matrix membranes, J. Appl. Pol. Sci., 101 (2006) 3800-3805.

[56] T.T. Moore, R. Mahajan, D.Q. Vu, W.J. Koros, Hybrid membrane materials comprising organic polymers with rigid dispersed phases, AIChE J., 50 (2004) 311-321.

[57] M. Hussain, A. König, Mixed-matrix membrane for gas separation: polydimethylsiloxane filled with zeolite, Chem. Eng. Technol., 35 (2012) 561-569.

[58] T.C. Merkel, R.P. Gupta, B.S. Turk, B.D. Freeman, Mixed-gas permeation of syngas components in poly(dimethylsiloxane) and poly(1-trimethylsilyl-1-propyne) at elevated temperatures, J. Membr. Sci., 191 (2001) 85-94.

[59] K. Friess, V. Hynek, M. Sipek, W.M. Kujawski, O. Vopicka, M. Zgazar, M.W. Kujawski, Permeation and sorption properties of poly(ether-block-amide) membranes filled by two types of zeolites, Sep. Purif. Technol., 80 (2011) 418-427.

[60] J. Ahn, W.-J. Chung, I. Pinnau, J. Song, N. Du, G.P. Robertson, M.D. Guiver, Gas transport behavior of mixed matrix membranes composed of silica nanoparticles in a polymer of intrinsic microporosity (PIM-1) J. Membr. Sci., 346 (2010) 280-287.

[61] D. Bastani, N. Esmaeili, M. Asadollahi, Polymeric mixed matrix membranes containing zeolites as a filler for gas separation applications: A review, J. Ind. Eng. Chem., 19 (2013) 375-393.

[62] H. Maghsoudi, M. Soltanieh, Simultaneous separation of H_2S and CO_2 from CH_4 by a high silica CHA-type zeolite membrane, J. Membr. Sci., 470 (2014) 159-165.

List of tables

List of figures

Figure 9. Relative CO_2/N_2 selectivity of the different MMM with respect to that of pure PTMSP membranes versus zeolite content at 298 K **a)** and 323 K **b).** CHA- (black), LTA5- (gray) and Rho- (light gray) based PTMSP MMM.